



1 Functional MRI brain state 2 occupancy in the presence of 3 cerebral small vessel disease – a 4 pre-registered replication analysis of 5 the Hamburg City Health Study

✉ For correspondence:
e.schlemm@uke.de

Present address:

Dr. Dr. Eckhard Schlemm,
Klinik und Poliklinik für
Neurologie,
Universitätsklinikum
Hamburg-Eppendorf,
Martinstr. 52,
D-20251 Hamburg

Data availability:

Preprocessed data is
available on
<https://github.com/csi-hamburg/HCHS-brain-states-RR>.

Funding: Hertie Network
of Excellence in Clinical
Neuroscience (Dr
Schlemm); Deutsche
Forschungsgemeinschaft
(DFG) – SFB 936,
178316478 – C2 (Drs
Thomalla & Cheng)

Competing interests: The
authors declare no
competing interests.

⁶ Thies Ingwersen, MD ¹, Carola Mayer, PhD ¹, Marvin Petersen, MD ¹,
⁷ Benedikt M. Frey, MD ¹, Jens Fiehler, MD ², Uta Hanning, MD ²,
⁸ Simone Kühn, PhD ^{3,4}, Jürgen Gallinat, MD ³, Raphael Twerenbold,
⁹ MD ⁵, Christian Gerloff, MD ⁶, Bastian Cheng, MD ¹, Götz Thomalla,
¹⁰ MD ¹, Eckhard Schlemm, MBBS PhD ¹✉

¹¹ Department of Neurology, University Medical Center
¹² Hamburg-Eppendorf; ¹³ Department of Neuroradiology, University
Medical Center Hamburg-Eppendorf; ¹⁴ Department of Psychiatry,
University Medical Center Hamburg-Eppendorf; ¹⁵ Max-Planck-Institut für
Bildungsforschung, Berlin; ¹⁶ Department of Cardiology, University
Medical Center Hamburg-Eppendorf; ¹⁷ University Medical Center
Hamburg-Eppendorf

¹⁸

¹⁹

20 Abstract

²¹ **Objective:** To replicate recent findings on the association between the extent of
²² cerebral small vessel disease (cSVD), functional brain network dedifferentiation, and
²³ cognitive impairment.

²⁴ **Methods:** We analyzed demographic, imaging, and behavioral data from the
²⁵ prospective population-based Hamburg City Health Study. Using a fully prespecified
²⁶ analysis pipeline, we estimated discrete brain states from structural and resting-state
²⁷ functional magnetic resonance imaging (MRI). In a multiverse analysis, we varied brain
²⁸ parcellations and functional MRI confound regression strategies. The severity of cSVD
²⁹ was operationalized as the volume of white matter hyperintensities of presumed
³⁰ vascular origin. Processing speed and executive dysfunction were quantified using the
³¹ Trail Making Test (TMT).

³² **Hypotheses:** We hypothesized a) that a greater volume of supratentorial white matter
³³ hyperintensities would be associated with less time spent in functional MRI-derived
³⁴ brain states of high fractional occupancy; and b) that less time spent in these
³⁵ high-occupancy brain states is associated with a longer time to completion in part B of
³⁶ the TMT.

³⁷ **Results:** High-occupancy brain states were characterized by activation or suppression
³⁸ of the default mode network. Every 5.1-fold increase in WMH volume was associated
³⁹ with a 0.94-fold reduction in the odds of occupying DMN-related brain states (P
⁴⁰ 5.01×10^{-8}). Every 5 % increase in time spent in high-occupancy brain states was
⁴¹ associated with a 0.98-fold reduction in the TMT-B completion time (P 0.0116). Findings
⁴² were robust across most brain parcellations and confound regression strategies.

⁴³ **Conclusion:** We successfully replicated previous findings on the association between
⁴⁴ cSVD, functional brain occupancy, and cognition in an independent sample. The data
⁴⁵ provide further evidence for a functional network dedifferentiation hypothesis of
⁴⁶ cSVD-related cognitive impairment. Further research is required to elucidate the
⁴⁷ mechanisms underlying these associations.

⁴⁸

⁴⁹ Introduction

⁵⁰ Cerebral small vessel disease (cSVD) is an arteriolopathy of the brain associated with age
⁵¹ and common cardiovascular risk factors (Wardlaw, C. Smith, and Dichgans, 2013). cSVD
⁵² predisposes patients to ischemic stroke (in particular lacunar stroke) and may lead to
⁵³ cognitive impairment and dementia (Cannistraro et al., 2019). Neuroimaging findings in
⁵⁴ cSVD reflect its underlying pathology (Wardlaw, Valdés Hernández, and Muñoz-Maniega,
⁵⁵ 2015) and include white matter hyperintensities (WMH), lacunes of presumed vascular

56 origin, small subcortical infarcts and microbleeds, enlarged perivascular spaces as well
57 as brain atrophy (Wardlaw, E. E. Smith, et al., 2013). However, the extent of visible cSVD
58 features on magnetic resonance imaging (MRI) is an imperfect predictor of the severity
59 of clinical sequelae (Das et al., 2019) and our understanding of the causal mechanisms
60 linking cSVD-associated brain damage to clinical deficits remains limited (Bos et al., 2018).

61 Recent efforts have focused on exploiting network aspects of the structural (Tuladhar,
62 Dijk, et al., 2016; Tuladhar, Tay, et al., 2020; Lawrence, Zeestraten, et al., 2018) and func-
63 tional (Dey et al., 2016; Schulz et al., 2021) organization of the brain to understand the
64 relationship between cSVD and clinical deficits in cognition and other domains that rely
65 on distributed processing. Reduced structural network efficiency has repeatedly been
66 described as a causal factor in the development of cognitive impairment, particularly
67 executive dysfunction and reduced processing speed in cSVD (Lawrence, Chung, et al.,
68 2014; Shen et al., 2020; Reijmer et al., 2016; Prins et al., 2005). Findings with respect
69 to functional connectivity (FC), however, are more heterogeneous than their SC counter-
70 parts, perhaps because FC measurements are prone to be affected by hemodynamic
71 factors and noise, resulting in relatively low reliability, especially with resting-state scans
72 of short duration (Laumann, Gordon, et al., 2015). This problem is exacerbated in the
73 presence of cSVD and worsened by arbitrary processing choices (Lawrence, Tozer, et al.,
74 2018; Gesierich et al., 2020).

75 As a promising new avenue, time-varying, or dynamic, functional connectivity approaches
76 have recently been explored in patients with subcortical ischemic vascular disease (Yin
77 et al., 2022; Xu et al., 2021). Although the study of dynamic FC measures may not solve
78 the problem of limited reliability, especially in small populations or participants with ex-
79 tensive structural brain changes, it adds another – temporal – dimension to the study of
80 functional brain organization, which is otherwise overlooked. Importantly, FC dynamics
81 not only reflect moment-to-moment fluctuations in cognitive processes, but are also re-
82 lated to brain plasticity and homeostasis (Laumann and Snyder, 2021; Laumann, Snyder,
83 et al., 2017), which may be impaired in cSVD.

84 In the present paper, we aimed to replicate and extend the main results of (Schlemm
85 et al., 2022). In this recent study, the authors analyzed MR imaging and clinical data from
86 the prospective Hamburg City Health Study (HCHS, (Jagodzinski et al., 2020)) using a coac-
87 tivation pattern approach to define discrete brain states and found associations between
88 the WMH load, time spent in high-occupancy brain states characterized by activation or

89 suppression of the default mode network (DMN), and cognitive impairment. Specifically,
90 every 4.7-fold increase in WMH volume was associated with a 0.95-fold reduction in the
91 odds of occupying a DMN-related brain state; every 2.5 seconds (i.e., one repetition time)
92 not spent in one of those states was associated with a 1.06-fold increase in TMT-B com-
93 pletion times.

94 The fractional occupancy of a functional MRI-derived discrete brain state is a participant-
95 specific measure of brain dynamics and is defined as the proportion of BOLD volumes
96 assigned to that state relative to all BOLD volumes acquired during a resting-state scan.

97 Our primary hypothesis for the present work was that the volume of supratentorial
98 white matter hyperintensities is associated with fractional occupancy of DMN-related
99 brain states in a middle-aged to elderly population mildly affected by cSVD. Our sec-
100 ondary hypothesis was that fractional occupancy is associated with executive dysfunc-
101 tion and reduced processing speed, measured as the time to complete part B of the Trail
102 Making Test (TMT).

103 Both hypotheses were tested in an independent subsample of the HCHS study popu-
104 lation using the same imaging protocols, examination procedures, and analysis pipelines
105 as those in (Schlemm et al., 2022). The robustness of the associations was explored using
106 a multiverse approach by varying key steps in the analysis pipeline.

107 Methods

108 Study population

109 This study analyzed data from the Hamburg City Health Study (HCHS), an ongoing prospec-
110 tive, population-based cohort study aiming to recruit a cross-sectional sample of 45 000
111 adult participants from the city of Hamburg, Germany (Jagodzinski et al., 2020). From
112 the first 10 000 participants of the HCHS, we planned to include those who were docu-
113 mented to have received brain imaging (n=2648) and exclude those who were analyzed
114 in our previous report (Schlemm et al., 2022) (n=970). The ethical review board of the
115 Landesärztekammer Hamburg (State of Hamburg Chamber of Medical Practitioners) ap-
116 proved the HCHS (PV5131), and all participants provided written informed consent.

117 Demographic and clinical characterization

118 From the study database, we extracted the participants' age at the time of inclusion in
119 years, their sex, and the number of years spent in education. During the visit to the study

¹²⁰ center, participants underwent cognitive assessment using standardized tests. From the
¹²¹ database, we extracted their performance scores on the Trail Making Test part B, mea-
¹²² sured in seconds, as an operationalization of executive function and psychomotor pro-
¹²³ cessing speed (Tombaugh, 2004; Arbuthnott and Frank, 2000). For descriptive purposes,
¹²⁴ we also extracted data on past medical history and reported the proportion of partici-
¹²⁵ pants with a previous diagnosis of dementia.

¹²⁶ MRI acquisition and preprocessing

¹²⁷ The magnetic resonance imaging protocol for the HCHS includes structural and resting-
¹²⁸ state functional sequences. The acquisition parameters for a 3 T Siemens Skyra MRI scan-
¹²⁹ ner (Siemens, Erlangen, Germany) have been previously reported (Petersen et al., 2020;
¹³⁰ Frey et al., 2021) and are given as follows:

¹³¹ For T_1 -weighted anatomical images, a 3D rapid acquisition gradient-echo sequence
¹³² (MPRAGE) was used with the following sequence parameters: repetition time TR = 2500 ms,
¹³³ echo time TE = 2.12 ms, 256 axial slices, slice thickness ST = 0.94 mm, and in-plane resolu-
¹³⁴ tion IPR = $(0.83 \times 0.83) \text{ mm}^2$.

¹³⁵ T_2 -weighted fluid attenuated inversion recovery (FLAIR) images were acquired with
¹³⁶ the following sequence parameters: TR = 4700 ms, TE = 392 ms, 192 axial slices, ST =
¹³⁷ 0.9 mm, IPR = $(0.75 \times 0.75) \text{ mm}^2$.

¹³⁸ 125 resting state functional MRI volumes were acquired (TR = 2500 ms; TE = 25 ms;
¹³⁹ flip angle = 90°; slices = 49; ST = 3 mm; slice gap = 0 mm; IPR = $(2.66 \times 2.66) \text{ mm}^2$). The
¹⁴⁰ participants were asked to keep their eyes open and to think of nothing.

¹⁴¹ We verified the presence and voxel dimensions of expected MRI data for each par-
¹⁴² ticipant and excluded those for whom at least one of T_1 -weighted, FLAIR, and resting-
¹⁴³ state MRI was missing. We also excluded participants with neuroradiologically confirmed
¹⁴⁴ space-occupying intra-axial lesion. To ensure reproducibility, no visual quality assess-
¹⁴⁵ ment of raw images was performed.

¹⁴⁶ For the remaining participants, structural and resting-state functional MRI data was
¹⁴⁷ preprocessed using FreeSurfer v6.0 (<https://surfer.nmr.mgh.harvard.edu/>), and fmriPrep
¹⁴⁸ v20.2.6 (Esteban et al., 2019), using default parameters. Participants were excluded if
¹⁴⁹ automated processing using at least one of these packages failed.

150 Quantification of WMH load

151 For our primary analysis, the extent of ischemic white matter disease was operational-
152 ized as the total volume of supratentorial WMHs obtained from automated segmentation
153 using a combination of anatomical priors, BIANCA (Griffanti, Zamboni, et al., 2016), and
154 LOCATE (Sundaresan et al., 2019), post-processed with a minimum cluster size of 30 vox-
155 els, as described in (Schlemm et al., 2022). In an exploratory analysis, we partitioned
156 voxels identified as WMH into deep and periventricular components according to their
157 distance to the ventricular system (cut-off 10 mm, (Griffanti, Jenkinson, et al., 2018))

158 Brain state estimation

159 The output from fMRIprep was post-processed using xcpEngine v1.2.3 to obtain de-confounded
160 spatially averaged BOLD time series (Ciric, Wolf, et al., 2017). For the primary analysis, we
161 used the $36p$ regression strategy and the Schaefer-400 parcellation (Schaefer et al., 2018),
162 as in (Schlemm et al., 2022).

163 Different atlases and confound regression strategies, as implemented in xcpEngine,
164 were included in an exploratory multiverse analysis.

165 Co-activation pattern (CAP) analysis was performed by first aggregating parcellated,
166 de-confounded BOLD signals into a ($n_{\text{parcels}} \times \sum_i n_{\text{time points},i}$) feature matrix, where $n_{\text{time points},i}$
167 denotes the number of retained volumes for participant i after confound regression.
168 Clustering was performed using the k -means algorithm ($k = 5$) with a distance measure
169 given by 1 minus the sample Pearson correlation between points, as implemented in
170 Matlab R2021a. We estimated the participant- and state-specific fractional occupancies,
171 which are defined as the proportion of BOLD volumes assigned to each brain state (Vi-
172 daurre et al., 2018). The two states with the highest average occupancies were identified
173 as the basis for further analysis.

174 Statistical analysis

175 For demographic (age, sex, and years of education) and clinical (TMT-B) variables, the
176 number of missing items is reported. For non-missing values, we provide descriptive
177 summary statistics using median and interquartile range. The proportions of men and
178 women in the sample are reported. Since we expected based on our pilot data (Schlemm
179 et al., 2022) that the proportion of missing data would be small, primary regression mod-
180 elling was carried out as a complete-case analysis.

181 As an outcome-neutral quality check of the implementation of the MRI processing
182 pipeline, brain state estimation, and co-activation pattern analysis, we compared frac-
183 tional occupancies between brain states. We expected that the average fractional oc-
184 cupancy in the two high-occupancy states would be higher than the average fractional
185 occupancy in the other three states. Point estimates and 95% confidence intervals are
186 presented for the difference in average fractional occupancy to verify this assertion.

187 For further analyses, non-zero WMH volumes were subjected to logarithmic transfor-
188 mation. Zero values retained their value of zero; to compensate, all models included a
189 binary indicator for zero WMH volume if at least one non-zero WMH value was present.

190 To assess the primary hypothesis of a negative association between the extent of
191 ischemic white matter disease and time spent in high-occupancy brain states, we per-
192 formed a fixed-dispersion Beta regression to model the logit of the conditional expec-
193 tation of the average fractional occupancy of two high-occupancy states as an affine
194 function of the logarithmized WMH load. Age and sex were included as covariates. The
195 strength of the association was quantified as the odds ratio per interquartile ratio of the
196 WMH burden distribution, and is accompanied by a 95% confidence interval. Significance
197 testing of the null hypothesis of no association was conducted at the conventional signif-
198 icance level of 0.05. Estimation and testing were carried out using the 'betareg' package
199 v3.1.4 in R v4.2.1.

200 To assess the secondary hypothesis of an association between time spent in high-
201 occupancy brain states and executive dysfunction, we performed a generalized linear
202 regression with a Gamma response distribution to model the logarithm of the condi-
203 tional expected completion time in part B of the TMT as an affine function of the average
204 fractional occupancy of two high-occupancy states. Age, sex, years of education, and
205 logarithmized WMH load were included as covariates. The strength of the association
206 was quantified as a multiplicative factor per percentage point and accompanied by a
207 95% confidence interval. Significance testing of the null hypothesis of no association was
208 conducted at the conventional significance level of 0.05. Estimation and testing were
209 performed using the glm function included in the 'stats' package from R v4.2.1.

210 Pre-registered analyses

211 The analysis plan was pre-registered on June 27 2023 at <https://osf.io/fcqmb>. The sample
212 size calculation was based on an effect size on the odds ratio scale of 0.95, correspond-
213 ing to an absolute difference in the probability of occupying a DMN-related brain state

214 between the first and third WMH-load quartile of 1.3 percentage points, and between
215 the 5% and 95% percentile of 3.1 percentage points. Approximating half the difference
216 in fractional occupancy of DMN-related states between different task demands (rest vs
217 n-back) in healthy participants, which was estimated to lie between 6 and 7 percentage
218 points (Cornblath et al., 2020), this value represented a plausible choice for the smallest
219 effect size of theoretical and practical interest. It also equals the estimated effect size
220 based on the data presented in (Schlemm et al., 2022).

221 Simple bootstrapping was used to create 10 000 hypothetical datasets of size 200, 400,
222 600, 800, 900, 910, ..., 1090, 1100, 1200, 1400, 1500, and 1600. Each dataset was then sub-
223 jected to the estimation procedure described above. For each sample size, the propor-
224 tion of datasets in which the primary null hypothesis of no association between fractional
225 occupancy and WMH load could be rejected at $\alpha = 0.05$ was computed and recorded as
226 a power curve in Figure 1.

227 A sample size of 960 would have allowed the replication of the reported effect with a
228 power of 80.2 %. We had anticipated a sample size of 1500, which would have yielded a
229 power of 93.9 %.

230 Multiverse analysis

231 In both (Schlemm et al., 2022) and our primary replication analysis, we made certain ana-
232 lytical choices in the operationalization of brain states and ischemic white matter disease,
233 namely the use of the 36p confound regression strategy, the Schaefer-400 parcellation,
234 and a BIANCA/LOCATE-based WMH segmentation algorithm. The robustness of the as-
235 sociation between WMH burden and time spent in high-occupancy states with regard to
236 other choices was explored in a multiverse analysis (Steegen et al., 2016). Specifically, in
237 an exploratory analysis, we estimated brain states from BOLD time series processed ac-
238 cording to a variety of established confound regression strategies and aggregated over
239 different cortical brain parcellations (Table 1, Ceric, Rosen, et al., 2018; Ceric, Wolf, et al.,
240 2017). The extent of cSVD was additionally quantified by the volume of deep and periven-
241 tricular white matter hyperintensities.

242 For each combination of analytical choice of confound regression strategy, parcella-
243 tion, and subdivision of white matter lesion load ($9 \times 9 \times 3 = 243$ scenarios in total), we
244 quantified the association between WMH load and average time spent in high-occupancy
245 brain states using odds ratios and 95 % confidence intervals as described above.

246 No hypothesis testing was performed for these multiverse analyses. Rather, they

247 serve to inform about the robustness of the outcome of the test of the primary hypothesis.
248 Any substantial conclusions about the association between the severity of cerebral
249 small vessel pathology and the time spent in high-occupancy brain states were drawn
250 from the primary analysis using pre-specified methodological choices, as stated in the
251 Scientific Question in Table 0.

252 **Further exploratory analysis**

253 In previous work, two high-occupancy brain states have been related to the default mode
254 network (Cornblath et al., 2020). We further explored this relationship by computing, for
255 each individual brain state, the cosine similarity of the positive and negative activations of
256 the cluster's centroid with a set of a priori defined functional 'communities' or networks
257 (Schaefer et al., 2018; Yeo et al., 2011). The results were visualized as spider plots for the
258 Schaefer atlases.

259 In further exploratory analyses, we describe the associations between brain state dynamics
260 and other measures of cognitive ability such as memory and language.

261 **Pilot data and analysis**

262 Summary data from the first 1000 imaging data points of the HCHS have been published
263 with (Schlemm et al., 2022) and formed the basis for the hypotheses tested in this replication
264 study. Before pre-registration, we had implemented our prespecified analysis pipeline
265 described above in R and Matlab, and applied it to this previous sample. Data, code
266 and results from this pilot analysis have been stored with the archived Stage 1 report on
267 GitHub (https://github.com/csi-hamburg/HCHS_brain_states_RR, v1.5) and preserved on
268 Zenodo.

269 **Timeline and access to data**

270 At the time of planning of this study, all demographic, clinical and imaging data used in
271 this analysis had been collected by the HCHS and were held in the central trial database.
272 Quality checks for non-imaging variables had been performed centrally. WMH segmentation
273 based on structural MRI data of the first 10 000 participants of the HCHS had been
274 performed previously using the BIANCA/LOCATE approach (Rimmele et al., 2022). Functional
275 MRI data and clinical measures of executive dysfunction (TMT-B scores) had not
276 previously been analyzed by the pre-registering author (ES).

277 Deviations from preregistration

278 For deconfounding and aggregating BOLD data at brain parcellation level, the software
279 xcpEngine was used in version 1.2.3, not 1.2.1, to ensure that the correct MNI ref-
280 erence template (MNI152NLin2009cAsym) is used for registration of brain atlases. This
281 decision was made before analysing the data.

282 Results

283 For this replication study, a total of 2648 datasets were available, of which 970 were al-
284 ready included in our previous analysis and thus discarded. In 13 of the resulting 1678
285 datasets, one or more MRI sequences were missing. Of the complete datasets (n=1665),
286 we excluded 5 participants due to intra-axial space-occupying lesions. An additional 9
287 participants were excluded because of unsuccessful preprocessing, WMH segmentation,
288 or xcpEngine failure, resulting in 1651 datasets for analysis. A study-flowchart is provided
289 in Figure 2.

290 Baseline demographic and cognitive values, including the number of missing items,
291 are reported in Table 3.

292 WMH volumes (median 1.05 mL, IQR 0.47 mL to 2.37 mL), motion estimates, and frac-
293 tional occupancies of brain states 1 through 5 are reported in Table 5.

294 In an outcome-neutral quality check of the implementation of (i) the MRI processing
295 pipeline, (ii) brain state estimation, and (iii) co-activation pattern analysis, the mean differ-
296 ence in fractional occupancy between high- and low-occupancy states was consistently
297 maintained, with a point-estimate of the separation between two high-occupancy and
298 three low-occupancy states of 6.7 % (95 % confidence interval, 6.2 % to 7.1 %) in the 36p
299 paradigm. This indicates that the implementation of the pipeline was correct and that
300 the brain state estimation and co-activation pattern analysis worked as intended.

301 Pre-registered hypotheses

302 Association between WMH load and fractional occupancy

303 The results of the test of our primary preregistered hypothesis of an association be-
304 tween supratentorial WMH volume and the time spent in high-occupancy brain states
305 are shown in Figure 3 and Table 7.

306 Adjusted for age and sex, there was a 0.94-fold reduction in the odds of occupying a
307 high-occupancy brain state for every 5.1-fold increase in WMH load ($P = 5.01 \times 10^{-8}$).

³⁰⁸ Association between executive function and fractional occupancy in DMN-related states

³¹⁰ The results of the test of our secondary preregistered hypothesis of an association be-
³¹¹ tween time spent in high-occupancy brain states and executive function as measured by
³¹² the complete part B of the TMT are shown in Figure 4 and Table 9.

³¹³ Adjusted for age, sex, WMH volume, and years of education, there was a 0.98-fold
³¹⁴ reduction in the time to complete the TMT-B for every 5 % increase in the time spent in
³¹⁵ high-occupancy brain states (P 0.0116).

³¹⁶ Multiverse analysis

³¹⁷ In a multiverse analysis, the main findings of associations between WMH load and FO
³¹⁸ and, to a lesser extent, between FO and TMT-B were robust with respect to the processing
³¹⁹ choices of brain parcellation and confound regression strategy.

³²⁰ A nominally statistically significant negative association between the total WMH load
³²¹ and time spent in high-occupancy states was observed in 48/81 scenarios, with 8/81 sig-
³²² nificant positive associations occurring with the Desikan–Killiany parcellation only (Fig-
³²³ ure 5A). For periventricular (deep) WMH volume, the results were similarly robust with
³²⁴ 49/81 (39/81) negative and 8/81 (0/81) positive associations of nominal statistical signifi-
³²⁵ cance, respectively.

³²⁶ The secondary finding of an association between greater TMT-B times and lower frac-
³²⁷ tional occupancy was less robust with only 16/81 nominally statistically significant neg-
³²⁸ ative and no significant positive associations, irrespective of operationalization of cSVD
³²⁹ (total vs. periventricular vs. deep WMH volume) (Figure 5B).

³³⁰ Additional analyses

³³¹ Connectivity profiles of brain states – relation to default mode network
³³² Based on the cosine similarity between positive and negative activations of cluster cen-
³³³ troids and indicator vectors of pre-defined large scale brain networks, network activation
³³⁴ profiles were computed for brain states estimated from Schaefer parcellations of varying
³³⁵ spatial resolutions.

³³⁶ Figure 6 shows the corresponding spider plots, identifying states characterized by
³³⁷ activation (DMN+) or suppression (DMN-) of the default mode network as states with the
³³⁸ highest fractional occupancy.

339 Association with other cognitive domains

340 Associations between the time spent in high-occupancy DMN-related brain states and
341 cognitive measures beyond TMT-B are shown in Figure 7.

342 Adjusted for age, sex, WMH load, and years of education, FO in DMN-related states
343 appeared to be associated with better word recall (adjusted OR 1.19, nominal P 0.013),
344 but not with global cognitive functioning (MMSE, adjusted OR 1.09) or vocabulary (aOR
345 1.09), nor with verbal fluency (animal naming, adjusted exp(β) 1.04), or pure processing
346 speed (TMT-A, adjusted exp(β) 0.97).

347 Summary and Discussion

348 In this pre-registered cross-sectional study we replicated the key findings of Schlemm
349 et al., 2022 in an independent population-based sample of 1651 middle-aged to elderly
350 participants of the Hamburg City Health Study.

351 First, we confirmed that the severity of cerebral small vessel disease is associated with
352 the time spent in high-occupancy brain states, defined by functional MRI. More precisely,
353 we showed that every 5.1-fold increase in the volume of supratentorial white matter hy-
354 perintensities of presumed vascular origin (WMH) was associated with a 0.95-fold reduc-
355 tion in the odds of occupying a brain state characterized by activation or suppression of
356 the default-mode network, at any given time during the resting-state scan.

357 Second, we confirmed that the time spent in high-occupancy brain states at rest is
358 associated with cognitive performance. More precisely, a 5%-reduction in the fractional
359 occupancy of DMN-related brain states was associated with a 1.02-fold increase in the
360 time to complete part B of the trail making test (TMT).

361 In a pre-planned multiverse analysis, findings relating to our primary and, to a lesser
362 extent, secondary hypotheses were robust with respect to variations in brain parcel-
363 lations and confound regression strategies. Inconsistent results were found with the
364 Desikan-Killiany parcellation, likely reflecting the notion that the spatial resolution and
365 functional specificity of this coarse, structurally defined atlas are inadequate for analyz-
366 ing functionally defined brain states. Across brain parcellations, effect sizes were smaller
367 with the ICA-AROMA confound regression strategy and failed to reach nominal statisti-
368 cal significance. This might be due to a relatively large residual motion component in
369 measures of dynamical functional Connectivity after de-noising with ICA-AROMA, as de-
370 scribed previously (Lydon-Staley et al., 2019).

³⁷¹ We also confirmed across several brain parcellation resolutions that high-occupancy
³⁷² states at rest are characterized by either activation or suppression of the default mode
³⁷³ network, reflecting its role as the predominant task-negative brain network.

³⁷⁴ In unplanned, exploratory analyses, we described the association between brain state
³⁷⁵ dynamics and cognitive measures other than executive function and processing speed
³⁷⁶ and reported a strong, preliminary association between time spent in high-occupancy
³⁷⁷ states and delayed word recall.

³⁷⁸ We further explored, and report in the Supplementary appendix, the effect of mo-
³⁷⁹ tion; results relating to our primary and, to a lesser extent, secondary, hypotheses were
³⁸⁰ robust to additional, unplanned adjustments for DVARS, RMSD, and mean framewise
³⁸¹ displacement.

³⁸² The presented results provide robust evidence for a behaviorally relevant association
³⁸³ between cerebral small vessel disease and functional brain network dedifferentiation.

³⁸⁴ Further research is required to replicate our findings in different populations, such
³⁸⁵ as those affected more severely by cSVD or cognitive impairment, or being studied using
³⁸⁶ different imaging protocols, to determine the generalizability of our findings with respect
³⁸⁷ to varying operationalizations of the notions of cSVD, brain state, and cognition, and to
³⁸⁸ understand the mechanisms underlying the reported associations.

³⁸⁹ Acknowledgment

³⁹⁰ This preprint was created using the LaPreprint template ([https://github.com/roaldarbol/](https://github.com/roaldarbol/lapreprint)
³⁹¹ [lapreprint](#)) by Mikkel Roald-Arbøl .

³⁹² Disclosure

³⁹³ The authors of this article declare that they have no financial conflict of interest with the
³⁹⁴ content of this article.

³⁹⁵ References

- ³⁹⁶ Arbuthnott, Katherine and Janis Frank (2000). "Trail making test, part B as a measure of
³⁹⁷ executive control: validation using a set-switching paradigm". In: *Journal of clinical and*
³⁹⁸ *experimental neuropsychology* 22.4, pp. 518–528.
- ³⁹⁹ Behzadi, Yashar et al. (2007). "A component based noise correction method (CompCor)
⁴⁰⁰ for BOLD and perfusion based fMRI". In: *Neuroimage* 37.1, pp. 90–101.

- ⁴⁰¹ Bos, Daniel et al. (2018). "Cerebral small vessel disease and the risk of dementia: A sys-
⁴⁰² tematic review and meta-analysis of population-based evidence". en. In: *Alzheimers.*
⁴⁰³ *Dement.* 14.11, pp. 1482–1492.
- ⁴⁰⁴ Cannistraro, Rocco J et al. (2019). "CNS small vessel disease: A clinical review". en. In: *Neu-*
⁴⁰⁵ *rology* 92.24, pp. 1146–1156.
- ⁴⁰⁶ Ceric, Rastko, Adon FG Rosen, et al. (2018). "Mitigating head motion artifact in functional
⁴⁰⁷ connectivity MRI". In: *Nature protocols* 13.12, pp. 2801–2826.
- ⁴⁰⁸ Ceric, Rastko, Daniel H Wolf, et al. (2017). "Benchmarking of participant-level confound
⁴⁰⁹ regression strategies for the control of motion artifact in studies of functional con-
⁴¹⁰ nectivity". en. In: *Neuroimage* 154, pp. 174–187.
- ⁴¹¹ Cornblath, Eli J et al. (2020). "Temporal sequences of brain activity at rest are constrained
⁴¹² by white matter structure and modulated by cognitive demands". en. In: *Commun Biol*
⁴¹³ 3.1, p. 261.
- ⁴¹⁴ Cox, Robert W (1996). "AFNI: software for analysis and visualization of functional mag-
⁴¹⁵ netic resonance neuroimages". In: *Computers and Biomedical research* 29.3, pp. 162–
⁴¹⁶ 173.
- ⁴¹⁷ Das, Alvin S et al. (2019). "Asymptomatic Cerebral Small Vessel Disease: Insights from
⁴¹⁸ Population-Based Studies". en. In: *J. Stroke Cerebrovasc. Dis.* 21.2, pp. 121–138.
- ⁴¹⁹ Desikan, Rahul S et al. (2006). "An automated labeling system for subdividing the human
⁴²⁰ cerebral cortex on MRI scans into gyral based regions of interest". In: *Neuroimage* 31.3,
⁴²¹ pp. 968–980.
- ⁴²² Dey, Ayan K et al. (2016). "Pathoconnectomics of cognitive impairment in small vessel
⁴²³ disease: A systematic review". en. In: *Alzheimers. Dement.* 12.7, pp. 831–845.
- ⁴²⁴ Esteban, Oscar et al. (2019). "fMRIprep: a robust preprocessing pipeline for functional
⁴²⁵ MRI". en. In: *Nat. Methods* 16.1, pp. 111–116.
- ⁴²⁶ Frey, Benedikt M et al. (2021). "White matter integrity and structural brain network topol-
⁴²⁷ ogy in cerebral small vessel disease: The Hamburg city health study". en. In: *Hum. Brain*
⁴²⁸ *Mapp.* 42.5, pp. 1406–1415.
- ⁴²⁹ Friston, Karl J et al. (1996). "Movement-related effects in fMRI time-series". In: *Magnetic*
⁴³⁰ *resonance in medicine* 35.3, pp. 346–355.
- ⁴³¹ Gesierich, Benno et al. (2020). "Alterations and test-retest reliability of functional connec-
⁴³² tivity network measures in cerebral small vessel disease". en. In: *Hum. Brain Mapp.*
⁴³³ 41.10, pp. 2629–2641.

- ⁴³⁴ Glasser, Matthew F et al. (2016). "A multi-modal parcellation of human cerebral cortex".
⁴³⁵ en. In: *Nature* 536.7615, pp. 171–178.
- ⁴³⁶ Gordon, Evan M et al. (2016). "Generation and Evaluation of a Cortical Area Parcellation
⁴³⁷ from Resting-State Correlations". en. In: *Cereb. Cortex* 26.1, pp. 288–303.
- ⁴³⁸ Griffanti, Ludovica, Mark Jenkinson, et al. (2018). "Classification and characterization of
⁴³⁹ periventricular and deep white matter hyperintensities on MRI: A study in older adults".
⁴⁴⁰ en. In: *Neuroimage* 170, pp. 174–181.
- ⁴⁴¹ Griffanti, Ludovica, Giovanna Zamboni, et al. (2016). "BIANCA (Brain Intensity AbNormal-
⁴⁴² ity Classification Algorithm): A new tool for automated segmentation of white matter
⁴⁴³ hyperintensities". en. In: *Neuroimage* 141, pp. 191–205.
- ⁴⁴⁴ Jagodzinski, Annika et al. (2020). "Rationale and Design of the Hamburg City Health Study".
⁴⁴⁵ en. In: *Eur. J. Epidemiol.* 35.2, pp. 169–181.
- ⁴⁴⁶ Laumann, Timothy O, Evan M Gordon, et al. (2015). "Functional system and areal organi-
⁴⁴⁷ zation of a highly sampled individual human brain". In: *Neuron* 87.3, pp. 657–670.
- ⁴⁴⁸ Laumann, Timothy O and Abraham Z Snyder (2021). "Brain activity is not only for thinking".
⁴⁴⁹ In: *Current Opinion in Behavioral Sciences* 40, pp. 130–136.
- ⁴⁵⁰ Laumann, Timothy O, Abraham Z Snyder, et al. (2017). "On the stability of BOLD fMRI
⁴⁵¹ correlations". In: *Cerebral cortex* 27.10, pp. 4719–4732.
- ⁴⁵² Lawrence, Andrew J, Ai Wern Chung, et al. (2014). "Structural network efficiency is as-
⁴⁵³ sociated with cognitive impairment in small-vessel disease". en. In: *Neurology* 83.4,
⁴⁵⁴ pp. 304–311.
- ⁴⁵⁵ Lawrence, Andrew J, Daniel J Tozer, et al. (2018). "A comparison of functional and trac-
⁴⁵⁶ tography based networks in cerebral small vessel disease". en. In: *Neuroimage Clin* 18,
⁴⁵⁷ pp. 425–432.
- ⁴⁵⁸ Lawrence, Andrew J, Eva A Zeestraten, et al. (2018). "Longitudinal decline in structural
⁴⁵⁹ networks predicts dementia in cerebral small vessel disease". en. In: *Neurology* 90.21,
⁴⁶⁰ e1898–e1910.
- ⁴⁶¹ Lydon-Staley, David M et al. (2019). "Evaluation of confound regression strategies for
⁴⁶² the mitigation of micromovement artifact in studies of dynamic resting-state func-
⁴⁶³ tional connectivity and multilayer network modularity". In: *Network Neuroscience* 3.2,
⁴⁶⁴ pp. 427–454.
- ⁴⁶⁵ Macey, Paul M et al. (2004). "A method for removal of global effects from fMRI time series".
⁴⁶⁶ In: *Neuroimage* 22.1, pp. 360–366.

- ⁴⁶⁷ Makris, Nikos et al. (2006). "Decreased volume of left and total anterior insular lobule in
⁴⁶⁸ schizophrenia". In: *Schizophrenia research* 83.2-3, pp. 155–171.
- ⁴⁶⁹ Muschelli, John et al. (2014). "Reduction of motion-related artifacts in resting state fMRI
⁴⁷⁰ using aCompCor". In: *Neuroimage* 96, pp. 22–35.
- ⁴⁷¹ Petersen, Marvin et al. (2020). "Network Localisation of White Matter Damage in Cerebral
⁴⁷² Small Vessel Disease". en. In: *Sci. Rep.* 10.1, p. 9210.
- ⁴⁷³ Power, Jonathan D, Alexander L Cohen, et al. (2011). "Functional network organization of
⁴⁷⁴ the human brain". en. In: *Neuron* 72.4, pp. 665–678.
- ⁴⁷⁵ Power, Jonathan D, Anish Mitra, et al. (2014). "Methods to detect, characterize, and re-
⁴⁷⁶ move motion artifact in resting state fMRI". In: *Neuroimage* 84, pp. 320–341.
- ⁴⁷⁷ Prins, Niels D et al. (2005). "Cerebral small-vessel disease and decline in information pro-
⁴⁷⁸ cessing speed, executive function and memory". en. In: *Brain* 128.Pt 9, pp. 2034–2041.
- ⁴⁷⁹ Pruim, Raimon HR et al. (2015). "ICA-AROMA: A robust ICA-based strategy for removing
⁴⁸⁰ motion artifacts from fMRI data". In: *Neuroimage* 112, pp. 267–277.
- ⁴⁸¹ Reijmer, Yael D et al. (2016). "Small vessel disease and cognitive impairment: The rele-
⁴⁸² vance of central network connections". en. In: *Hum. Brain Mapp.* 37.7, pp. 2446–2454.
- ⁴⁸³ Rimmeli, David Leander et al. (2022). "Association of Carotid Plaque and Flow Velocity
⁴⁸⁴ With White Matter Integrity in a Middle-aged to Elderly Population". en. In: *Neurology*.
- ⁴⁸⁵ Satterthwaite, Theodore D et al. (2013). "An improved framework for confound regres-
⁴⁸⁶ sion and filtering for control of motion artifact in the preprocessing of resting-state
⁴⁸⁷ functional connectivity data". In: *Neuroimage* 64, pp. 240–256.
- ⁴⁸⁸ Schaefer, Alexander et al. (2018). "Local-Global Parcellation of the Human Cerebral Cortex
⁴⁸⁹ from Intrinsic Functional Connectivity MRI". en. In: *Cereb. Cortex* 28.9, pp. 3095–3114.
- ⁴⁹⁰ Schlemm, Eckhard et al. (2022). "Equalization of Brain State Occupancy Accompanies
⁴⁹¹ Cognitive Impairment in Cerebral Small Vessel Disease". en. In: *Biol. Psychiatry* 92.7,
⁴⁹² pp. 592–602.
- ⁴⁹³ Schulz, Maximilian et al. (2021). "Functional connectivity changes in cerebral small vessel
⁴⁹⁴ disease - a systematic review of the resting-state MRI literature". en. In: *BMC Med.* 19.1,
⁴⁹⁵ p. 103.
- ⁴⁹⁶ Shen, Jun et al. (2020). "Network Efficiency Mediates the Relationship Between Vascular
⁴⁹⁷ Burden and Cognitive Impairment: A Diffusion Tensor Imaging Study in UK Biobank".
⁴⁹⁸ en. In: *Stroke* 51.6, pp. 1682–1689.

- ⁴⁹⁹ Steegen, Sara et al. (2016). "Increasing Transparency Through a Multiverse Analysis". en.
⁵⁰⁰ In: *Perspect. Psychol. Sci.* 11.5, pp. 702–712.
- ⁵⁰¹ Sundaresan, Vaanathi et al. (2019). "Automated lesion segmentation with BIANCA: Im-
⁵⁰² pact of population-level features, classification algorithm and locally adaptive thresh-
⁵⁰³ olding". en. In: *Neuroimage* 202, p. 116056.
- ⁵⁰⁴ Tombaugh, Tom N (2004). "Trail Making Test A and B: normative data stratified by age
⁵⁰⁵ and education". en. In: *Arch. Clin. Neuropsychol.* 19.2, pp. 203–214.
- ⁵⁰⁶ Tuladhar, Anil M, Ewoud van Dijk, et al. (2016). "Structural network connectivity and cog-
⁵⁰⁷ nition in cerebral small vessel disease". en. In: *Hum. Brain Mapp.* 37.1, pp. 300–310.
- ⁵⁰⁸ Tuladhar, Anil M, Jonathan Tay, et al. (2020). "Structural network changes in cerebral small
⁵⁰⁹ vessel disease". en. In: *J. Neurol. Neurosurg. Psychiatry* 91.2, pp. 196–203.
- ⁵¹⁰ Tzourio-Mazoyer, Nathalie et al. (2002). "Automated anatomical labeling of activations in
⁵¹¹ SPM using a macroscopic anatomical parcellation of the MNI MRI single-subject brain".
⁵¹² In: *Neuroimage* 15.1, pp. 273–289.
- ⁵¹³ Vidaurre, Diego et al. (2018). "Discovering dynamic brain networks from big data in rest
⁵¹⁴ and task". en. In: *Neuroimage* 180.Pt B, pp. 646–656.
- ⁵¹⁵ Wardlaw, Joanna M, Colin Smith, and Martin Dichgans (2013). "Mechanisms of sporadic
⁵¹⁶ cerebral small vessel disease: insights from neuroimaging". en. In: *Lancet Neurol.* 12.5,
⁵¹⁷ pp. 483–497.
- ⁵¹⁸ Wardlaw, Joanna M, Eric E Smith, et al. (2013). "Neuroimaging standards for research
⁵¹⁹ into small vessel disease and its contribution to ageing and neurodegeneration". en.
⁵²⁰ In: *Lancet Neurol.* 12.8, pp. 822–838.
- ⁵²¹ Wardlaw, Joanna M, María C Valdés Hernández, and Susana Muñoz-Maniega (2015). "What
⁵²² are white matter hyperintensities made of? Relevance to vascular cognitive impair-
⁵²³ ment". en. In: *J. Am. Heart Assoc.* 4.6, p. 001140.
- ⁵²⁴ Xu, Yuanhang et al. (2021). "Altered Dynamic Functional Connectivity in Subcortical Is-
⁵²⁵ chemic Vascular Disease With Cognitive Impairment". en. In: *Front. Aging Neurosci.* 13,
⁵²⁶ p. 758137.
- ⁵²⁷ Yeo, B T Thomas et al. (2011). "The organization of the human cerebral cortex estimated
⁵²⁸ by intrinsic functional connectivity". en. In: *J. Neurophysiol.* 106.3, pp. 1125–1165.
- ⁵²⁹ Yin, Wenwen et al. (2022). "The Clustering Analysis of Time Properties in Patients With
⁵³⁰ Cerebral Small Vessel Disease: A Dynamic Connectivity Study". en. In: *Front. Neurol.*
⁵³¹ 13, p. 913241.

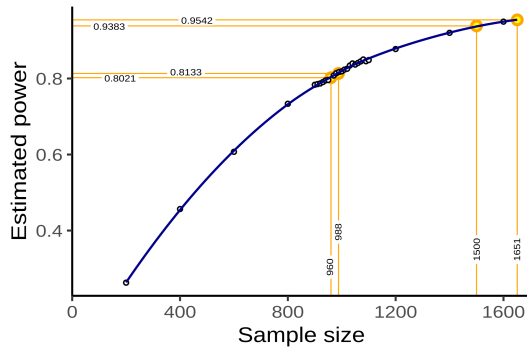


Figure 1 | Sample size and power estimation. A-priori estimated power for different sample sizes was obtained as the proportion of synthetic data sets in which the null hypothesis of no association between WMH volume and time spent in high-occupancy brain states can be rejected at the $\alpha = 0.05$ significance level. Proportions are based on a total of 10 000 synthetic data sets obtained by bootstrapping the data presented in (Schlemm et al., 2022). Highlighted in orange are the smallest sample size ensuring a power of at least 80 % ($n = 960$), the sample size of the pilot data ($n = 988$, post-hoc power 81.3 %), the expected sample size for this replication study ($n = 1500$, a-priori power 93.9 %), and the achieved sample size ($n = 1651$, a-priori power 95.4 %).

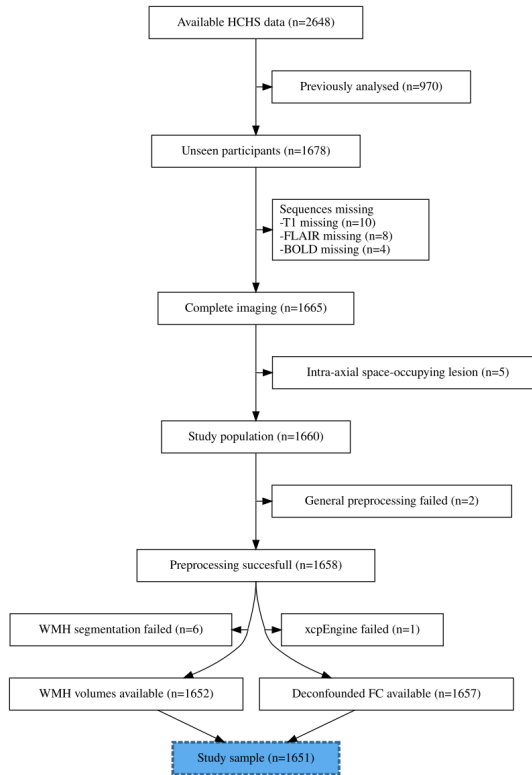


Figure 2 | Study flowchart. Composition of the study population after application of inclusion and exclusion criteria, and image processing.

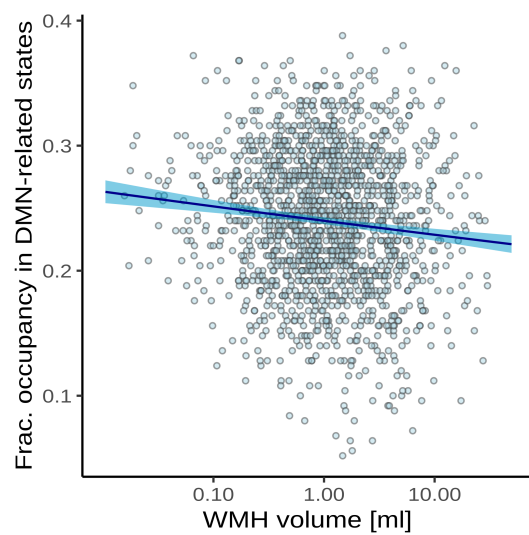


Figure 3 | Association between time spent in high-occupancy brain states and supratentorial WMH volume. Point estimates (black line) and 95%-confidence region (light blue ribbon) of the conditional mean fractional occupancy are obtained from unadjusted beta regression modelling. Each marker represents one of N=1642 independent participants with a non-zero total WMH volume.

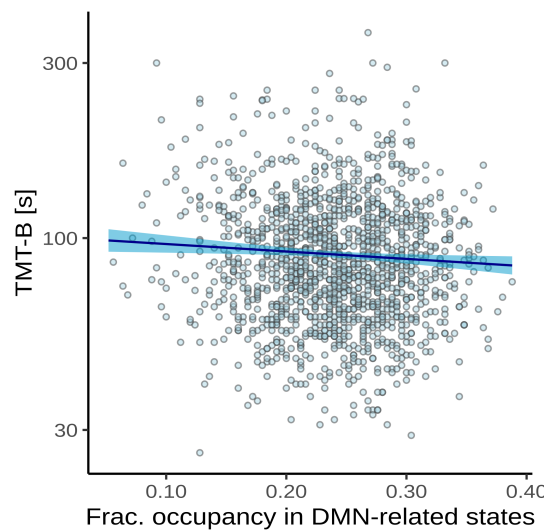


Figure 4 | Association between time spent in high-occupancy DMN-related brain states and TMT-B completion time. Point estimates (black line) and 95%-confidence region (light blue ribbon) of the conditional mean TMT-B completion time are obtained from unadjusted Gamma regression modelling. Each marker represent one of N=1482 independent participants with non-zero total WMH volume and available TMT-B data.

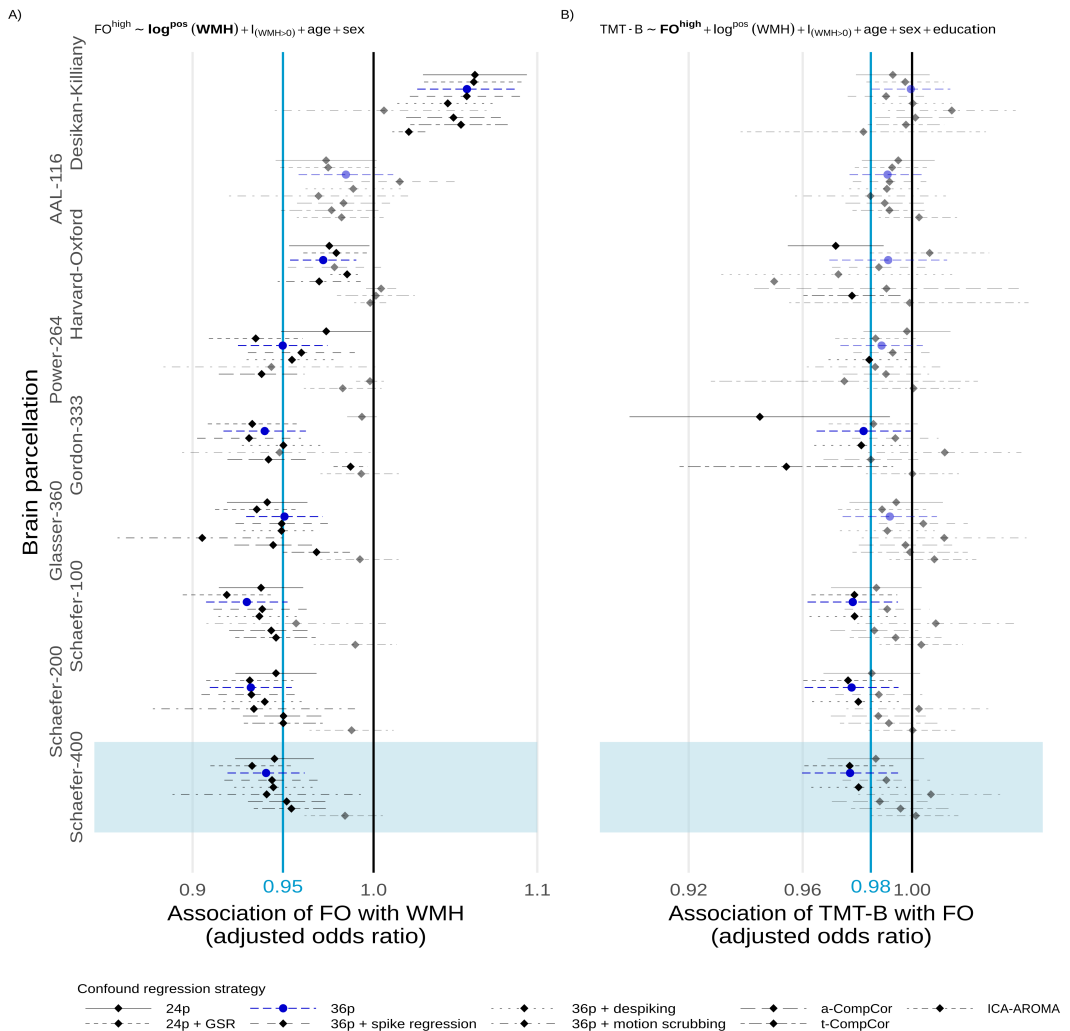


Figure 5 | Multiverse analysis. Adjusted effect size estimates of the associations between cSVD severity (WMH volume) and network dedifferentiation (less time spent in high-occupancy DMN-related brain states) [A]), and between network dedifferentiation and executive function (TMT-B completion time) [B]). Effect sizes are given per 5.1-fold increase in WMH volume and a 5%-increase in fractional occupancy, respectively. Markers and line segments indicate point estimates and 95%-confidence intervals for adjusted odds ratios for different combinations of confound regression strategy and brain parcellation. The primary analytical choices are indicated by dark blue circles (36p) and light blue shading (Schaefer-400). Model equations for beta and gamma regressions, respectively, are given at the top. Vertical lines indicate no effect (black) and the effect size observed in the discovery cohort (Schlemm et al., 2022) (light blue), respectively, for reference. Effect sizes not reaching nominal statistical significance ($\alpha = 0.05$) are shown desaturated. Corresponding data based on periventricular and deep WMH volumes are presented in the Supplementary Appendix.

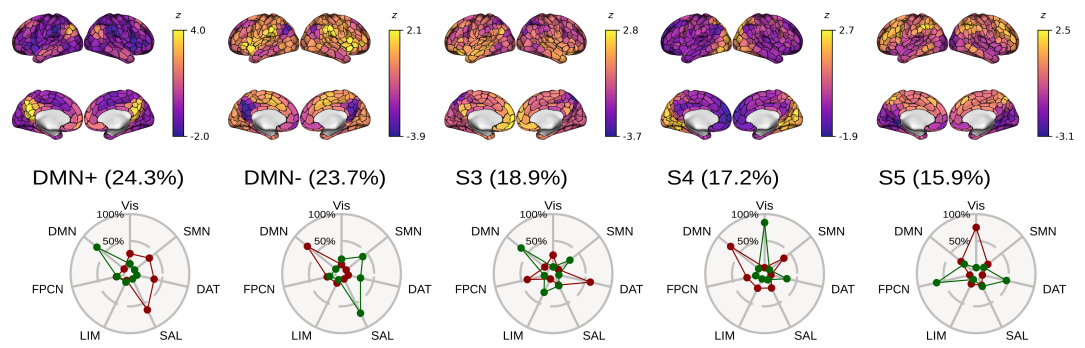


Figure 6 | Connectivity profiles of brain states. [Top] Centroids of each identified brain state visualized in brain space. Note the individual color scales. [Bottom] Cosine similarity between centroids of brain states and signed indicator vectors corresponding to activation (green) and suppression (red) of each of seven predefined large-scale functional brain networks (Yeo et al., 2011).

States are ordered by mean fractional occupancy across N=1651 independent participants, indicated by parenthetical percentages. Two high-occupancy states are characterized by activation or suppression of the DMN, the remaining three low-occupancy states (S3–5) were not used in the present study. Note that mean FO values are similar, but not identical, to median FO values reported in Table 5.

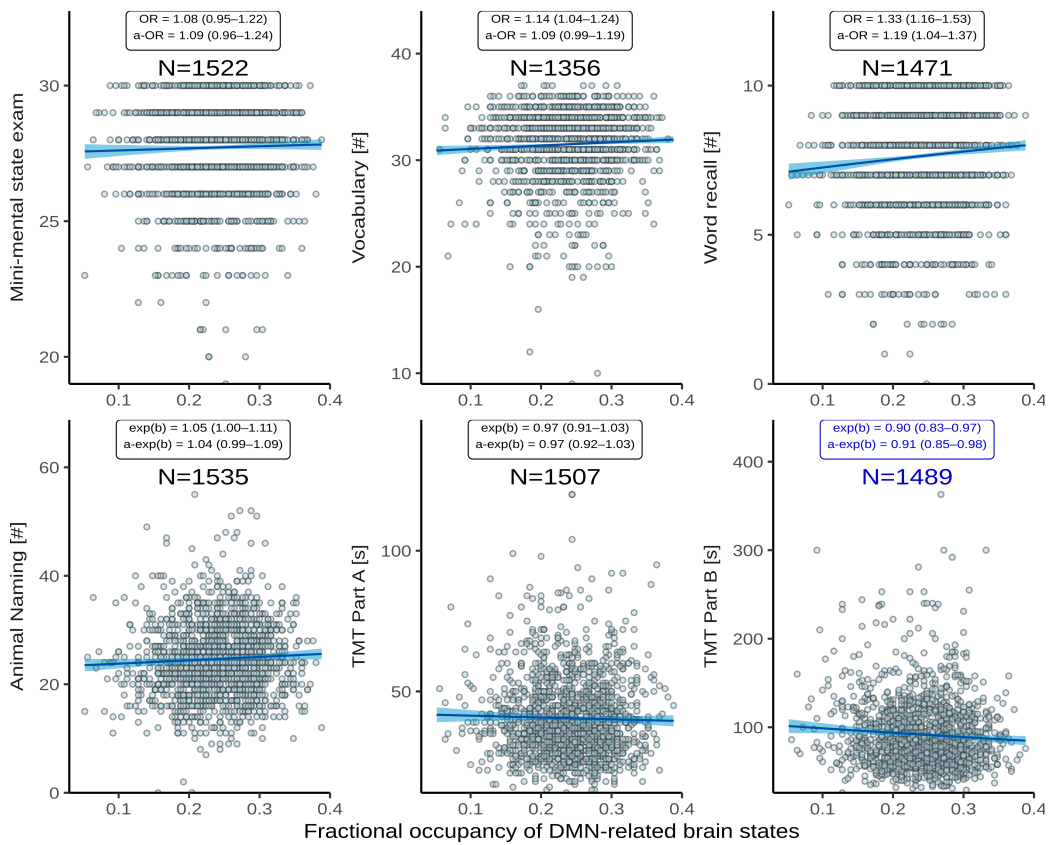


Figure 7 | Association between time spent in high-occupancy DMN-related brain states and cognitive measures. Point estimates (black line) and 95%-confidence region (light blue ribbon) of the conditional mean cognitive measures are obtained from unadjusted binomial (top row: Mini-Mental State Examination, Vocabulary, Word List Recall, logit link) and Gamma regression (bottom row: Animal Naming, Trail Making Test [TMT] A/B: log link) modelling. Each marker represents one of N independent participants, as indicated. Insets report effect sizes and P-values both with (adjusted [a-]) and without adjustment for the nuisance variables age, sex, WMH volume (coded as in Figure 5), and years of education. Effect sizes were quantified as odds ratios (ORs) (top) or response scale multipliers [exp(b)] (bottom), and correspond to a 20%-increase in fractional occupancy. Note the different reference change in FO compared to Table 9 chosen to adequately represent some of the smaller effect sizes. The bottom right panel highlighted in dark blue reproduces Figure 4.

Question	Hypothesis	Sampling plan	Analysis plan	Ratio- nale for decid- ing the sensitiv- ity of the test	Interpretation given different outcomes	Theory that could be shown wrong by the outcome
Is severity of cerebral small disease, quantified by the volume of supratentorial white matter hyperintensities of presumed vascular origin (WMH), associated with time spent in high-occupancy brain states, defined by resting-state functional MRI?	(Primary) Higher WMH volume is associated with lower average occupancy of the two highest-occupancy brain states.	Available participants with clinical and imaging data from the HCHS (Jagodzinski et al., 2020)	Standardized preprocessing of structural and functional MRI data • automatic quantification of WMH • co-activation pattern analysis • multivariable generalised regression analyses	Tradition	$P < 0.05 \rightarrow$ rejection of the null hypothesis of no association between cSVD and fractional occupancy; $P > 0.05 \rightarrow$ insufficient evidence to reject the null hypothesis	Functional brain dynamics are not related to subcortical ischemic vascular disease.
Is time spent in high-occupancy brain states associated with cognitive impairment, measured as the time to complete part B of the trail making test (TMT)?	(Secondary) Lower average occupancy of the two highest-occupancy brain states is associated with longer TMT-B time.	as above	as above	as above	$P < 0.05 \rightarrow$ rejection of the null hypothesis of no association between fractional occupancy and cognitive impairment; $P > 0.05 \rightarrow$ insufficient evidence to reject the null hypothesis	Cognitive function is not related to MRI-derived functional brain dynamics.

Table 0 | Study Design Template. Overview of the Scientific Questions addressed in the present study (first column), the two main hypotheses being investigated (second column), and details of the underlying study.

Name of the atlas	#parcels	Reference
Desikan-Killiany	86	Desikan et al., 2006
AAL	116	Tzourio-Mazoyer et al., 2002
Harvard-Oxford	112	Makris et al., 2006
glasser360	360	Glasser et al., 2016
gordon333	333	Gordon et al., 2016
power264	264	Power, Cohen, et al., 2011
schaefer{N}	100	Schaefer et al., 2018
	200	
	400	

AAL: Automatic Anatomical Labelling

(a) Parcellations

Design	Reference
24p	Friston et al., 1996
24p + GSR	Macey et al., 2004
36p	Satterthwaite et al., 2013
36p + spike regression	Cox, 1996
36p + despiking	Satterthwaite et al., 2013
36p + scrubbing	Power, Mitra, et al., 2014
aCompCor	Muschelli et al., 2014
tCompCor	Behzadi et al., 2007
AROMA	Pruim et al., 2015

GSR: Global signal regression, AROMA: Automatic Removal of Motion Artifacts

(b) Confound regression strategies, adapted from (Ciric, Wolf, et al., 2017)

Table 1 | Multiverse analysis. Overview over different brain parcellations and confound regression strategies implemented using xcpEngine (Ciric, Rosen, et al., 2018). A total of $9 \times 9 = 81$ analytical combinations were explored to assess the robustness of our results with respect to these processing choices.

N = 1,651	
<i>Demographics (no Missing n (%))</i>	
Age, yr	
Median (IQR)	66 (59 – 72)
Sex	
Male	940/1651 (57%)
Female	711/1651 (43%)
<i>Cardiovascular risk factors</i>	
Hypertension	
Present	1177/1611 (73.1%)
Missing n (%)	85 (5.1%)
Diabetes	
Present	157/1566 (10%)
Missing n (%)	40 (2.4%)
Smoking	
Present	200/1360 (14.7%)
Missing n (%)	201 (12.9%)
Hyperlipidaemia	
Present	426/1578 (27%)
Missing n (%)	73 (4.4%)
<i>Cognitive test results</i>	
MMSE, # (max. 30)	
Median (IQR)	28 (27 – 29)
Missing n (%)	129 (7.8%)
Vocabulary (MWT-B), # (max. 37)	
Median (IQR)	32 (30 – 34)
Missing n (%)	295 (18%)
Word recall, # (max. 10)	
Median (IQR)	8 (6 – 9)
Missing n (%)	180 (11%)
Animal Naming	
Median (IQR)	24 (20 – 29)
Missing n (%)	116 (7.0%)
TMT-A, seconds	
Median (IQR)	38 (31 – 48)
Missing n (%)	144 (8.7%)
TMT-B, seconds	
Median (IQR)	83 (65 – 110)
Missing n (%)	162 (9.8%)
<i>History</i>	
Diagnosed dementia	
Present	6/1645 (0.4%)
Missing n (%)	6 (0.4%)
Years of education	
Median (IQR)	13 (12 – 16)
Missing n (%)	34 (2%)

Table 3 | Descriptive statistics of the study population. Data are presented as median (interquartile range) or count (percentage) of non-missing items, as appropriate. Number of percentage of missing items are reported separately.

N = 1,651	
WMH volume ¹ , mL	
Total	1.05 (0.47 – 2.37), 9 Z
Periventricular	0.94 (0.43 – 2.04), 9 Z
Deep	0.10 (0.03 – 0.37), 344 Z
Motion during rs-fMRI	
Framewise displacement, mm	0.21 (0.15 – 0.63)
RMSD, mm	0.086 (0.058 – 0.12)
DVARS	27.8 (24.3 – 31.8)
Fractional occupancy, %	
DMN+	24.8 (20.8 – 28.0)
DMN-	24.0 (20.0 – 28.0)
S3	18.4 (15.2 – 22.4)
S4	16.8 (12.8 – 20.8)
S5	15.2 (12.0 – 19.2)

¹Number of zero values indicated by Z

Table 5 | Structural and functional imaging characteristics. Data are presented as median (interquartile range). Supratentorial WMH volumes were obtained by semiautomatic segmentation of FLAIR images using a BINACA/LOCATE-based *k*-nearest neighbours algorithm and stratified by their distance to the lateral ventricles (<10 mm, periventricular; >10 mm, deep). Motion parameters were estimated during fMRIprep processing of BOLD scans. Fractional occupancies were calculated by assigning individual BOLD volumes to one of five discrete brain states defined by k-means clustering-based co-activation pattern analysis. Two high-occupancy states are labelled DMN+ and DMN- in view of their network connectivity profiles as shown in Figure 6.

	Estimate	P	95%-CI
Intercept	0.24	<0.0001	0.21 – 0.27
WMH, per 5.1-fold increase ¹	0.94	<0.0001	0.92 – 0.96
Age, per 10 years	1.04	0.001	1.01 – 1.06
Female sex	1.12	<0.0001	1.09 – 1.16
$\mathbf{1}_{\{\text{WMH}=0\}}$	0.93	0.477	0.75 – 1.14

¹ Interquartile ratio 2.37/0.468 = 5.06

Table 7 | Association between time-spent in high-occupancy DMN-related brain states and WMH volume adjusted for age and sex. Beta regression table estimated from $n = 1651$ independent participants using the model equation $\text{FO}^{\text{high}} \sim \log \text{WMH}^+ + \mathbf{1}_{\{\text{WMH}=0\}} + \text{age} + \text{sex}$.

	Estimate	P	95%-CI
Intercept	53.41	< 0.0001	42.7 – 66.8
FO ^{high} , per 5%	0.98	0.0116	0.96 – 0.99
WMH, per 5.1-fold increase ¹	1.01	0.367	0.98 – 1.05
Age, per 10 years	1.18	<0.0001	1.15 – 1.21
Female sex	0.99	0.666	0.95 – 1.03
Education, per year	0.97	<0.0001	0.97 – 0.98
1_{WMH=0}	0.97	0.398	0.92 – 1.03

¹ Interquartile ratio 2.37/0.468 = 5.06

Table 9 | Association between TMT-B and time spent in high-occupancy DMN-related brain states adjusted for age, sex, WMH volume and years of education. Gamma regression table

estimated from $n = 1483$ independent participants using the model equation

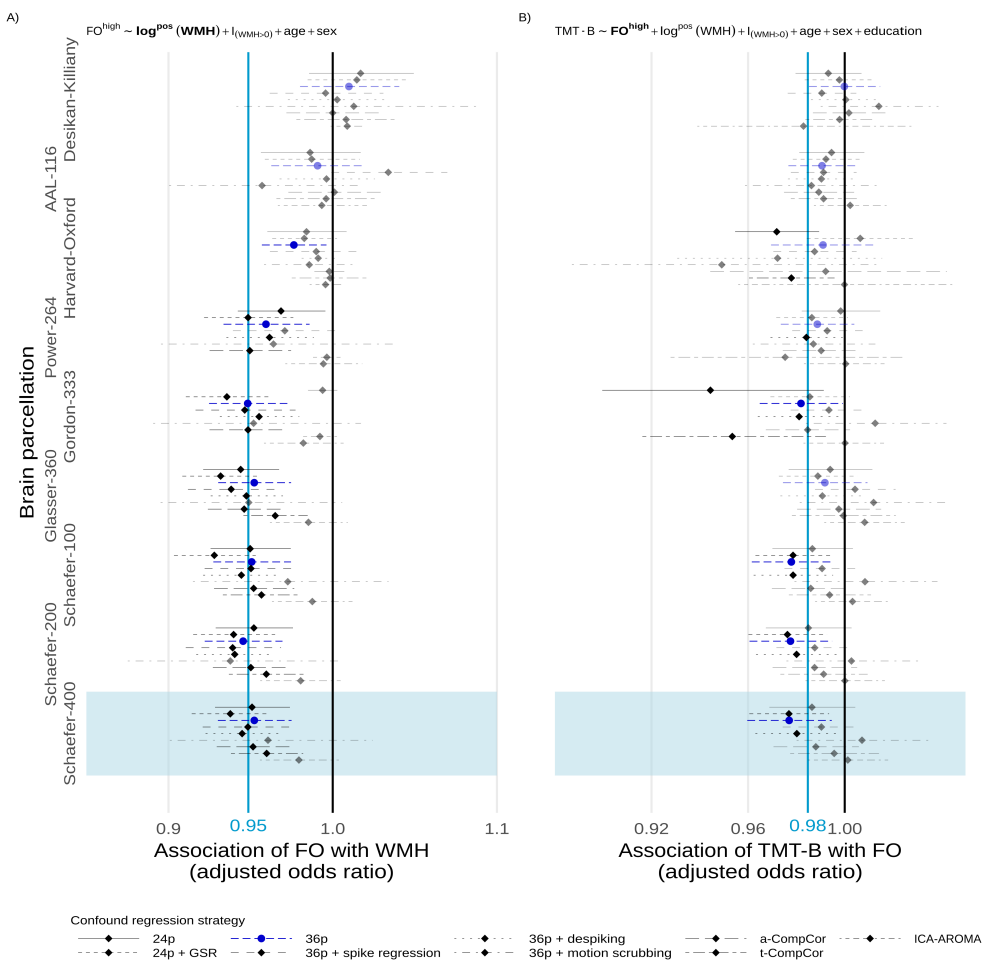
$TMT-B \sim FO^{high} + \log WMH^+ + 1_{\{WMH=0\}} + \text{age} + \text{sex} + \text{educationyears}$.

Appendix 1

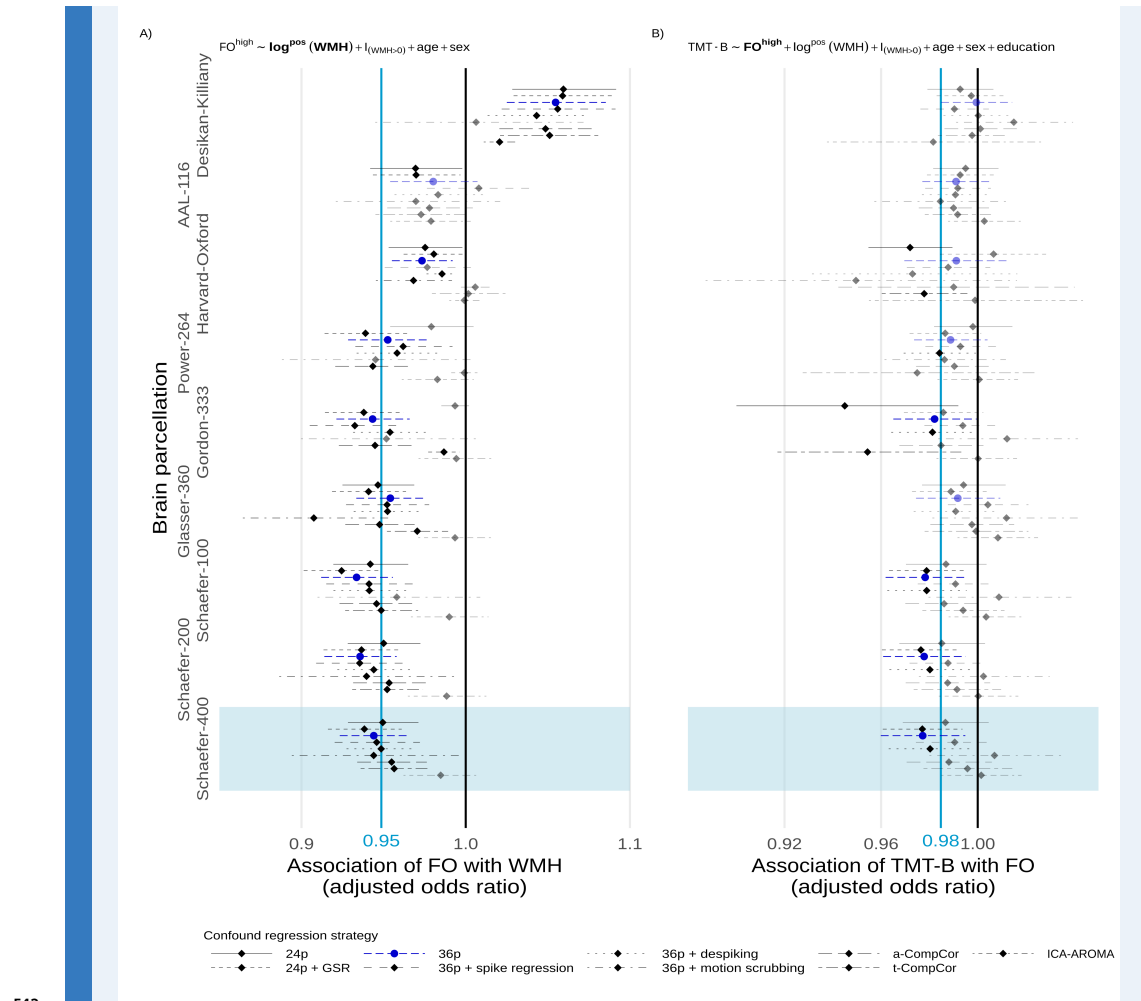
Supplementary results

Deep and periventricular WMH

Here we present, in analogy to Figure 5, the results of the multiverse analyses of the association between cSVD burden, FO of DMN-related states, and executive function, when cSVD is operationalized as the volume of deep or periventricular white matter hyperintensities, respectively.



Appendix 1—figure 1 Multiverse analysis, deep WMH



Appendix 1—figure 2 Multiverse analysis, periventricular WMH

545

Motion parameters

546

We also present, in analogy to Tables 7 and 9, regression tables for the association between time spent in DMN-related brain states (FO) and WMH volume, and between TMT-B and FO, adjusted for DVARS, RSMD and framewise displacement, in addition to age, sex and, in the latter case, years of education.

547

548

549

	Estimate	P	95%-CI
Intercept	0.32	<0.0001	0.28 – 0.36
WMH, per 5.1-fold increase ¹	0.96	0.0004	0.94 – 0.98
Age, per 10 years	1.01	<0.0001	1.00 – 1.01
Female sex	1.11	<0.0001	1.08 – 1.15
$\mathbf{1}_{\{\text{WMH}=0\}}$	0.91	0.3552	0.74 – 1.11

DVARS	0.98	<0.0001	0.98 – 0.99
RMSD	28.29	0.0055	2.67 – 299.84
Framewise displacement	0.16	0.0112	0.04 – 0.66

⁵⁵⁰ ⁵⁵¹ ⁵⁵² ⁵⁵³ ¹ Interquartile ratio 2.37/0.468 = 5.06

Appendix 1—table 2 Association between time-spent in high-occupancy DMN-related brain states and WMH volume adjusted for age, sex, and **motion parameters**

	Estimate	P	95%-CI
Intercept	46.83	<0.0001	36.74 – 59.72
FO ^{high} , per 5%	0.71	0.0718	0.49 – 1.03
WMH, per 5.1-fold increase ¹	1.01	0.3414	0.98 – 1.04
Age, per 10 years	1.02	<0.0001	1.01 – 1.02
Female sex	1.00	0.8171	0.96 – 1.04
Education, per year	0.97	<0.0001	0.97 – 0.98
1 _{WMH=0}	0.96	0.7581	0.73 – 1.29
DVARS	1.01	0.0001	1.00 – 1.01
RMSD	0.31	0.4695	0.01 – 7.45
Framewise displacement	1.08	0.9322	0.16 – 7.13

⁵⁵⁴ ⁵⁵⁵ ⁵⁵⁶ ⁵⁵⁷ ⁵⁵⁸ ¹ Interquartile ratio 2.37/0.468 = 5.06

Appendix 1—table 4 Association between TMT-B and time spent in high-occupancy DMN-related brain states adjusted for age, sex, WMH volume and years of education, and **motion parameters**